Exosome-mediated release of bis(monoacylglycerol)phosphate is regulated by LRRK2 and Glucocerebrosidase activity

Elsa Meneses-Salas, PhD,[1] Marianna Arnold,[2] Frank Hsieh, PhD,[2] Carlos Enrich, PhD,[1] Suzanne R. Pfeffer, PhD,[3,4] Kalpana Merchant, PhD,[5,*] and Albert Lu MD, PhD,[1*]

[1]Departament de Biomedicina, Unitat de Biologia Cel·lular, Facultat de Medicina i Ciències de la Salut, Centre de Recerca Biomèdica CELLEX, Institut d'Investigacions Biomèdiques August Pi i Sunyer, Universitat de Barcelona, Barcelona, Spain.

[2]NextCea Inc., Woburn, MA, USA

[3]Department of Biochemistry, Stanford University, Stanford CA, USA 94305-5307

[4]Aligning Science Across Parkinson's (ASAP) Collaborative Research Network, Chevy Chase, MD, USA

[5]Department of Neurology, Northwestern University, Chicago, IL, USA

[*]To whom correspondence should be addressed. E-mail: albertlu@ub.edu or kalpana kalpana.merchant@northwestern.edu

Address:

C/ Casanova 143

08036 Barcelona

SPAIN

phone: +34 93 227 5400 ext. 3358

FAX: +34 93 402 1907

KEYWORDS:

Parkinson's disease; bis(monoacyglycerol)phosphate; Endo-lysosomes; Exosomes; Extracellular vesicles

ABBREVIATIONS:

BMP, bis(monoacyglycerol)phosphate; CBE, conduritol β-epoxide; DHA, docosahexaenoic acid; GCase, glucocerebrosidase; ILV, intralumenal vesicle; LBPA, Lysobisphosphatidic acid; LRRK2, leucine-rich repeat kinase 2; PD, Parkinson's disease; WT, wild type

ABSTRACT

Background:

The endo-lysosomal phospholipid, bis(monoacylglycerol)phosphate (BMP), is aberrantly high in the urine of Parkinson's patients with mutations in genes encoding leucine-rich repeat kinase 2 (LRRK2) and glucocerebrosidase (GCase). Because BMP resides on and regulates the biogenesis of endo-lysosomal intralumenal membranes (exosomes when released), we hypothesized that elevated urinary BMP may be driven by increased exocytosis of BMP-enriched exosomes.

Objective:

Our aim was to explore the contribution of LRRK2 and GCase activities in the regulation of BMP metabolism and release.

Methods:

Microscopy and biochemical assays were used to analyze antibody-accessible BMP and exosome release in wild type (WT) and R1441G LRRK2–expressing mouse embryonic fibroblast cells. Lipidomics analysis was conducted to measure BMP and lipid content in cells and isolated exosomes. In these experiments, we tested the effects of LRRK2 and GCase inhibitors, MLi-2 and conduritol β-epoxide respectively, to assess regulation of BMP by LRRK2 and GCase.

Results:

Alterations in antibody-accessible BMP and endo-lysosome morphology were detected in R1441G LRRK2 cells. Lipidomics analysis revealed increased BMP content in mutant LRRK2 MEFs compared to WT MEFs. Inhibition of LRRK2 partially restored cellular and exosome-associated BMP levels; abrogation of GCase activity had the opposite effect. Metabolic labeling experiments confirmed that BMP synthesis is not influenced by LRRK2 or GCase activities. Pharmacological modulation of exosome release further confirmed exosome-mediated BMP exocytosis.

Conclusions:

LRRK2 regulates BMP in cells and its release in exosomes, which can be further modulated by GCase activity. These results have implications for the use of exosomal BMP as a Parkinson's disease biomarker.

INTRODUCTION

Variants in the gene encoding Leucine rich repeat kinase 2 (*LRRK2*) and β-glucocerebrosidase (GCase; *GBA1*) together constitute the largest contributors to familial and sporadic Parkinson's disease (PD)[1]. Although *LRRK2* G2019S is the most prevalent PD mutation, R1441G *LRRK2* is more penetrant and is associated with an earlier disease onset[2-4]. A shared mechanism of pathogenesis among all PD-causing

LRRK2 mutations is increased LRRK2 kinase activity, which leads to hyper-phosphorylation of its cognate substrates, Rab GTPases, including Rab8, Rab10 and Rab12, that are key regulators of intracellular vesicle trafficking[5]. A prevailing hypothesis of pathogenesis in LRRK2 PD cases is that LRRK2 phosphorylation of Rabs results in defective autophagy and endo-lysosomal homeostasis and defective ciliogenesis in the nigrostriatal circuit[5,6].

In contrast to LRRK2, the mechanism by which *GBA1* variants cause PD is less clear, although a role in alpha-synuclein aggregation and clearance has been proposed[7,8]. *GBA1* encodes a lysosomal hydrolase, glucocerebrosidase (GCase), essential for glycosphingolipid degradation. Homozygous loss-of-function mutations in *GBA1* cause Gaucher's disease, a lysosomal storage disorder characterized by cytotoxic accumulation of lipid substrates of GCase, glucosylceramide and glucosylsphingosine whereas heterozygous carriers have a 5-10 fold increased risk of PD [9,10]. Additionally, we and others previously showed that GCase enzymatic function is modulated by LRRK2 kinase activity[11,12]. Altogether, it is possible that dysregulation of the endo-lysosomal biology is associated with pathogenic variants of *LRRK2* and *GBA1*[6,13].

Bis(monoacylglycerol)phosphate (BMP, also known as LBPA or Lysobisphosphatidic acid) is an atypical, negatively-charged glycerophospholipid important for maintaining endo-lysosomal homeostasis[14]. BMP resides primarily in endo-lysosomal intralumenal vesicles (ILVs) where it participates in multiple processes, including cholesterol egress, exosome biogenesis and lipid catabolism[14,15]. Of note, BMP acts together with Saposin-C as enzymatic cofactors of GCase[16,17]. Multiple BMP isomers are present in cells, based on differences in their fatty acyl chains and their positions relative to the sn-2 and sn-3 carbon atoms on each of its two glycerol backbones[14,15]; the sn-2:sn-2' isomer is the proposed active form[18,19]. Dioleoyl-BMP (di-18:1-BMP) is the predominant form in numerous cell lines analyzed[20-23] and didocosahexaenoyl-BMP (di-22:6-BMP) is one of the most abundant species in the brain[24,25]. Fatty acyl composition is thought to influence BMP biophysical properties and function[26].

We and others recently reported elevated levels of di-18:1-BMP and di-22:6-BMP species in the urine of carriers of *LRRK2* and *GBA1* mutations[27-29]. Although we did not observe a correlation between urinary BMP and PD progression[28], these studies underscore BMP's potential diagnostic value and utility as a target modulation biomarker in therapeutic trials. Based on our previous findings, in the present study we focused on these two BMP species.

Given the specific intracellular localization of BMP (in ILVs; exosomes when released) and its proposed roles in exosome biogenesis[19], we hypothesized that its increased levels in PD biofluids may be a consequence of upregulated exosome secretion. To gain mechanistic insight into the regulation and biological significance of BMP release, we monitored BMP release in exosomes and performed kinetic analyses of BMP biosynthesis in mouse embryonic fibroblasts (MEFs) from wild-type (WT) or R1441G LRRK2 knock-in mice. In addition, we examined the regulation of BMP by a LRRK2 kinase inhibitor, MLi2, and a GCase inhibitor, conduritol β-epoxide (CBE), to garner insights into the role of BMP in potential therapeutic vs. pathophysiological responses, respectively. Our data indicate that LRRK2 and GCase activities do not alter BMP synthesis rates but instead modulate its release in CD63-positive exosomes.

RESULTS

Analysis of BMP-positive endo-lysosomes in R1441G LRRK2 mouse embryonic fibroblasts

We first performed a general immunofluorescence microscopy analysis of BMP-positive endo-lysosomes in both WT and R1441G LRRK2 knock-in MEFs. We found that the overall antibody-accessible BMP pool was significantly lower in mutant LRRK2-expressing cells compared to WT (Figure 1A, B). In contrast, endo-lysosomal LAMP2 fluorescence was higher in mutant LRRK2 MEFs (Figure 1A, C). Previous studies found structural defects in endo-lysosomes of different cell types harboring pathogenic LRRK2 mutations[30-32]. Since BMP is specifically enriched in ILVs present in the lumen of endo-lysosomes where it regulates important catabolic reactions, we examined multivesicular endosome (MVE) morphology of these cells. In agreement with previous findings[32], transmission electron microscopy revealed decreased MVE area in R1441G LRRK2 MEFs (average area= 0.11 μm^2) compared to WT MEFs (average area= 0.27 μm^2) (Figure 1D, E). In addition, the overall endo-lysosomal ILV number was diminished in the R1441G LRRK2 cell line (Figure 1F). These data suggest that the pathogenic LRRK2 mutation alters BMP-positive endo-lysosomes.

LRRK2 and GCase activities modulate exosome release

Given the previously described roles of BMP in ILV/exosome biogenesis, we investigated whether the alterations observed in antibody-accessible BMP and MVE ILV number in LRRK2 mutant MEFs could be reflected by changes in exosome release. We isolated and characterized exosomes from both WT and R1441G MEFs and also assessed the effects of LRRK2 and GCase pharmacological inhibitors, MLi-2 and CBE, respectively. Inhibition of LRRK2 kinase and GCase enzymatic activities was confirmed, respectively, by monitoring phopsho-Rab10 levels in whole cell lysates and performing a fluorescence-based GCase activity assay in cells (Figure 2A, B). Consistent with our immunofluorescence data,

upregulation of LAMP2 was observed in R1441G LRRK2 whole cell lysates (WCL; Figure 2 A, C, D and E), as previously reported in LRRK2 G2019S knock-in mouse brain[33]. MLi-2 treatment partially reversed this phenotype (Figure 2 A, C, E), suggesting that aberrant LRRK2 kinase activity influences endo-lysosomal homeostasis. Biochemical analysis of exosomal fractions revealed elevation of LAMP2, but not Flotillin-1 levels in R1441G LRRK2 MEF-derived exosomes compared to WT MEFs (Figure 2 C). This apparent discrepancy may reflect differences in molecularly distinct exosomal subpopulations[34,35] released by the WT and mutant cells. Nevertheless, analysis of WT cell-derived exosomes revealed no major differences in exosomal marker levels between untreated (control) and MLi-2- or CBE-treated conditions (Supplemental Figure 1A-C). Interestingly, a modest but significant decrease in exosome-associated protein markers was observed upon MLi-2 treatment in isolated exosomal fractions from mutant LRRK2 MEFs (Figure 2C, F, G). In contrast, inhibition of GCase activity in mutant LRRK2 cells resulted in the opposite effect on LAMP2-positive exosome release. (Figure 2D, G). Given the enrichment of LAMP2 in exosomes rather than ectosomes (released by outward budding from the plasma membrane) [35], these results suggest that exosome secretion is influenced by LRRK2 kinase and GCase hydrolase activities; while MLi-2 treatment decreased exosome release, CBE increased it.

Targeted BMP lipid analysis in intact cells and exosomes

We used ultra-performance liquid chromatography-tandem mass spectrometry (UPLC-MS/MS) to measure quantitatively the impact of LRRK2 and GCase activities on BMP isoform abundance in cells and isolated exosomal fractions. Remarkably, an overall increase in total BMP isoforms was detected in mutant LRRK2 MEF cell lysates (Figure 3A-D), with di-22:6-BMP and di-18:1-BMP as the major species. It is important to note that mass spec methods detect total BMP content while antibody staining (Figure 1) only detects so-called “antibody-accessible” BMP[36]. The mass spectrometry-based increase in total BMP in LRRK2 mutant cells indicates that this pool is less antibody-accessible than that present in wild type cells.

LRRK2 inhibition for 48 hours with MLi-2 slightly decreased total di-22:6-BMP and total di-18:1-BMP levels in R1441G LRRK2 cells (Figure 3A and B). Conversely, inhibition of GCase increased di-22:6-BMP levels compared with untreated, R1441G LRRK2 cells (Figure 3C and D). No statistically significant differences in intracellular BMP levels were observed in WT LRRK2 MEFs upon LRRK2 or GCase inhibition (Supplemental Figure 1D, E), suggesting a dominant role of mutant LRRK2 activity in BMP regulation. Targeted quantification of sphingolipid species confirmed inhibition of GCase activity in both CBE-treated WT and mutant LRRK2 cells. GCase substrates were more elevated in CBE-treated

R1441G LRRK2 than in WT cells, suggesting broader endo-lysosome dysfunction (Supplemental Figure 2A).

Analysis of isolated exosomal fractions revealed increased BMP content in WT MEF-derived exosomes compared with R1441G LRRK2 MEFs (Figure 3E). However, no significant differences in exosome-associated BMP abundance between untreated (control) and MLi-2- or CBE-treated WT LRRK2 MEFs were observed (Supplemental Figure 1F). These data suggest LRRK2-independent clonal differences in basal BMP release.

A significant partial decrease in exosome-associated BMP was detected upon MLi-2 treatment of LRRK2 R1441G MEFs (Figure 3E), consistent with previous observations in non-human primates and PD mouse models that showed decreased extracellular urinary BMP upon LRRK2 kinase pharmacological inhibition[37-39]. In contrast, interfering with GCase activity resulted an opposite, albeit not significant, trend (Figure 3E). These later results may be explained by incomplete GCase inhibition in LRRK2 R1441G cells (Figure 2B). Finally, exosome-associated GCase substrates (glucosylceramide, galactosylceramide, glucosylsphingosine) were lower in R1441G LRRK2 cells compared with WT MEFs, but no significant differences were detected between control or CBE-treated conditions independent of LRRK2 mutation status (except for glucosylsphingosine, which showed an increase in WT-exosomes upon GCase inhibition; Supplemental Figure 2B). Given that BMP specifically resides in ILVs (exosomes upon release), these data together with our previous biochemical analysis (Figure 2C, D, F) suggest a role for LRRK2 and GCase in up-modulating BMP release in association with LAMP2-positive exosomes from MEF cells.

BMP biosynthesis is not influenced by LRRK2 kinase and GCase activities

To rule out the possibility that differences in cellular and exosome-associated BMP levels following MLi-2 or CBE treatment of R1441G cells were caused by alterations in BMP metabolism rather than changes in membrane trafficking and exosome release, we performed metabolic labeling experiments using heavy (H) isotope-labeled 22:6 and 18:1 fatty acids as BMP precursors.

Cells were pulsed with heavy isotope BMP precursors and then washed and chased for different time points (Figure 4A). UPLC-MS/MS analysis allowed us to differentiate unlabeled versus semi-labeled (H,L'; only one heavy isotope-labeled fatty acid chain) or fully-labeled (H,H'; both fatty acid chains heavy isotope-labeled) BMP species (Figure 4A). Initial experiments were performed over 48h using mutant LRRK2 cells under control and LRRK2- or GCase-inhibition conditions; untreated WT cells were

included for comparison. Strikingly, even at time 0 and throughout the length of the experiment, R1441G LRRK2 cells displayed substantially higher H,L'- and H,H'-22:6-BMP species than WT cells (left and middle plots in Figure 4 B). H,L', but not H,H' 18:1-BMP was detected, which appeared to increase to a greater extent in R1441G LRRK2 cells at least during the initial 8h of the experiment (right plot, Figure 4 B). Despite these differences between WT and mutant LRRK2 cells, neither inhibition of LRRK2 or GCase had a major impact in the kinetics of BMP synthesis or catabolism (Figure 4B). To better resolve initial BMP synthesis rates, we reduced the pulse labeling time and chase time to 60 min. In this set of experiments, only isotope-labeled 22:6-BMP species were detected (Figure 4C), possibly reflecting a preference for 22:6 BMP synthesis by MEFs. As before, even at time 0 and throughout the 60 min duration of the assay, 22:6-BMP levels were consistently higher in R1441G LRRK2 cells compared with WT MEFs. Again, no overall differences were seen between untreated and MLi-2- or CBE-treated cells. These experiments support the hypothesis that rather than altering BMP metabolic rates, LRRK2 and GCase activities influence exosome-mediated BMP release.

BMP release is exosome-mediated

Our data suggest that BMP is exocytosed in association with exosomes and that LRRK2 and GCase activities modulate BMP secretion. To determine the magnitude of BMP release via exosome secretion, we assessed the impact of pharmacological modulators of exosome release. Treatment of WT MEFs with GW4869, a selective type 2-neutral sphingomyelinase inhibitor, significantly decreased exosomal BMP levels (Figure 5A, B). On the other hand, enhancing exosome release with bafilomycin A1 (B-A1), a pharmacological inhibitor of the endo-lysosomal proton pump V-ATPase that dramatically boosts exosome exocytosis[35,40], resulted in the opposite trend (Figure 3A, C). Biochemical analysis of exosome release in R1441G LRRK2 cells showed similar behavior as in WT MEFs upon treatment with these pharmacological agents (Figure 5A and Supplemental Figure 3). Consistent with the data obtained from isolated exosomal fractions, while GW4869 increased cellular BMP content (Figure 5D), B-A1 diminished intracellular total di-22:6-BMP and di-18:1-BMP (Figure 5E). Altogether, these results strongly support the notion that BMP is released by exosome-mediated MVE exocytosis.

DISCUSSSION

Here we have shown that hyperactive LRRK2 kinase upregulates BMP levels in MEF cells and the exosomes that they release. Moreover, LRRK2 and GCase pharmacological inhibitors, MLi-2 and CBE, modulate BMP abundance in cells and isolated exosomal fractions in opposite direction without interfering with the kinetics of BMP biosynthetic or catabolic rates. While PD-associated mutations in *LRRK2* cause an increase in kinase activity, *GBA1* pathogenic variants are associated with decreased

GCase enzymatic function. Therefore, MLi-2 treatment represents a potential therapeutic rescue, whereas CBE phenocopies pathogenic conditions. Accordingly, effects of MLi-2 and CBE were in opposite directions in our biochemical and lipidomics analysis data. Finally, BMP release was modulated by pharmacological agents known to modify exosome secretion. Together, these data provide novel insights into the mechanisms that control BMP metabolism in cells and are consistent with dysregulated exocytosis of BMP-containing exosomes, accounting for anomalous extracellular BMP levels detected in the urine of PD cases.

Despite its discovery in the late nineteen sixties[41], very little is known about BMP's metabolic regulation in cells. Pioneering studies by Gruenberg and colleagues underscored the importance of BMP in endo-lysosome homeostastic regulation and generation of endo-lysosomal ILVs[14,18,19] that become exosomes upon release. Subsequent studies showed that cellular levels of this atypical phospholipid are invariably altered in many neurodegenerative disorders characterized by endo-lysosome dysfunction[24]. We and others reported that BMP is aberrantly high in urine derived from LRRK2 and GBA mutation-carriers[27-29]. These results have also been reproduced in animal models, in which urinary BMP levels decrease upon administration of MLi-2 and other LRRK2 kinase inhibitors[37-39]. The present study complements these previous observations by providing a mechanism of BMP release that can be regulated by LRRK2 and GCase enzymatic activity.

Our microscopy analysis reveals decreased antibody-accessible BMP levels in R1441G LRRK2 cells. In contrast, our targeted lipid pathway analysis measurements consistently show higher total BMP levels in R1441G LRRK2 cells compared with WT cells. As we have reported previously[36], BMP antibody detects only a sub-pool of "accessible" BMP while mass spectrometry detects all pools. Given the essential roles of BMP in endo-lysosomal catabolism, our immunofluorescence data predict that LRRK2 mutant cells have defective degradative capacity, consistent with recent reports[30,42]. In addition, we found a concomitant upregulation of LAMP2 in R1441G LRRK2 MEFs (Figure 1A, C; Figure 2A, C, D, E), suggesting that LRRK2 may participate in endo-lysome biogenesis regulation[42].

BMP is enriched in urinary exosomes[43]. However, other studies did not detect BMP enrichment in isolated exosomes and concluded that BMP may be present in ILVs of endo-lysosomal subpopulations devoted to degradative activities rather than exocytic events[44,45], as previously proposed[46]. Using our UPLC-MS/MS methodology, extracellular BMP can be efficiently detected in the urine of healthy and mutant LRRK2/GCase carriers[27-29], and additionally, in exosomal fractions derived from both WT and R1441G LRRK2 MEFs (this study).

How does LRRK2 influence release of BMP-positive exosomes? A subset of Rab proteins that are master regulators of intracellular membrane trafficking pathways are important LRRK2 substrates[5]. Some of these Rabs include Rab10, Rab12 and Rab35, and have been shown to play regulatory roles in endo-lysosomal exocytosis and exosome release[47,48]. We thus speculate that phosphorylation of one or several of these Rabs may lead to enhanced BMP release. Indeed, G2019S LRRK2-–mediated Rab35 phosphorylation has been proposed to promote exosome-mediated α-synuclein release and propagation between cells[49,50]. In addition, aberrant LRRK2 and GCase activities may trigger endo-lysosomal exocytosis, and associated release of BMP-containing exosomes, via a so-called clearance pathway activated due to accumulation of cytotoxic endo-lysosomal substrates[51,52]. The contribution of these phosphorylated Rabs to exosome-mediated BMP release will be of interest for future work.

In summary, this work provides evidence that LRRK2 and GCase pathological activities upregulate exosome-mediated BMP release without altering its metabolism in cells. MLi2-mediated changes Our findings suggest that exocytosis of BMP-positive exosomes is driven by aberrant LRRK2 and GCase activities. What is the clinical significance of elevated urinary BMP levels in PD patients? Inhibition of LRRK2 improves endo-lysosomal function[42], this is consistent with increased LRRK2 and decreased GCases activities associated with pathogenic variants which worsen endo-lysosomal homeostasis[6,13]; this may eventually lead to endo-lysosomal exocytosis followed by exosome-mediate BMP release. We speculate that BMP-exosomes may harbor a distinct molecular repertoire that could perhaps inform more precisely disease progression or pathobiology. Future investigations will be needed to study the contribution of dysfunctional LRRK2 and GCase in exocytosis of specific BMP-positive endo-lysosomal subpopulations and to further characterize the role of BMP-positive exosomes in the context of disease pathophysiology but also as a PD diagnostic tool.

ACKNOWLEDGMENTS

This research was funded by a grant to K.M and A.L from The Michael J. Fox Foundation for Parkinson's Research (MJFF-019043).

AUTHOR CONTRIBUTIONS

K.M.M. and A.L. conceived the project with input from F.H. All experiments were carried out by E.M-S. and A.L. except for mass spectrometric analysis of BMP (F.H). C.E. captured and analyzed transmission electron microscopy images. K.M., A.L., S.R.P. and F.H. oversaw the project. K.M. and A.L.

obtained research funding. A.L. wrote and edited the manuscript with critical review/revision from all co-authors.

COMPETING INTERESTS

Following authors declare no competing non-financial interests but the following competing financial interests: Kalpana M. Merchant, PhD, has consulted for AcureX, Caraway, Nitrase, Nura Bio, Retromer Therapeutics, Sinopia Biosciences, Vanqua, Vida Ventures and the Michael J. Fox Foundation for Parkinson's Research. She has received research funding from the Michael J. Fox Foundation for Parkinson's Research. Albert Lu, MD, PhD, and Suzanne R. Pfeffer, Ph.D. have received research funding from the Michael J. Fox Foundation for Parkinson's Research. Frank Hsieh, PhD is employed by Nextcea, Inc., which holds patent rights to the di-22:6-BMP and 2,2'-di-22:6-BMP biomarkers for neurological diseases involving lysosomal dysfunction (US 8,313,949, Japan 5,702,363, and Europe EP2419742).

REFERENCES

1. Smith LJ, Lee CY, Menozzi E, Schapira AHV. Genetic variations in GBA1 and LRRK2 genes: Biochemical and clinical consequences in Parkinson disease. Front Neurol. 2022;13:971252. doi:10.3389/fneur.2022.971252
2. Yue Z, Lachenmayer ML. Genetic LRRK2 models of Parkinson's disease: Dissecting the pathogenic pathway and exploring clinical applications. Mov Disord. 2011;26(8):1386-1397. doi:10.1002/mds.23737
3. Pont-Sunyer C, Tolosa E, Caspell-Garcia C, et al. The prodromal phase of leucine-rich repeat kinase 2-associated Parkinson disease: Clinical and imaging Studies. Mov Disord. 2017;32(5):726-738. doi:10.1002/mds.26964
4. Fan Y, Nirujogi RS, Garrido A, et al. R1441G but not G2019S mutation enhances LRRK2 mediated Rab10 phosphorylation in human peripheral blood neutrophils. Acta Neuropathol. 2021;142(3):475-494. doi:10.1007/s00401-021-02325-z
5. Pfeffer SR. LRRK2 phosphorylation of Rab GTPases in Parkinson's disease. FEBS Lett. 2022;10.1002/1873-3468.14492. doi:10.1002/1873-3468.14492
6. Roosen DA, Cookson MR. LRRK2 at the interface of autophagosomes, endosomes and lysosomes. Mol Neurodegener. 2016;11(1):73. doi:10.1186/s13024-016-0140-1
7. Fredriksen K, Aivazidis S, Sharma K, et al. Pathological α-syn aggregation is mediated by glycosphingolipid chain length and the physiological state of α-syn in vivo. Proc Natl Acad Sci U S A. 2021;118(50):e2108489118. doi:10.1073/pnas.2108489118

8. Stojkovska I, Wani WY, Zunke F, et al. Rescue of α-synuclein aggregation in Parkinson's patient neurons by synergistic enhancement of ER proteostasis and protein trafficking. Neuron. 2022;110(3):436-451.e11. doi:10.1016/j.neuron.2021.10.032
9. Sidransky E, Lopez G. The link between the GBA gene and parkinsonism. Lancet Neurol. 2012;11(11):986-998. doi:10.1016/S1474-4422(12)70190-4
10. Duran R, Mencacci NE, Angeli AV, et al. The glucocerobrosidase E326K variant predisposes to Parkinson's disease, but does not cause Gaucher's disease. Mov Disord. 2013;28(2):232-236. doi:10.1002/mds.25248
11. Ysselstein D, Nguyen M, Young TJ, et al. LRRK2 kinase activity regulates lysosomal glucocerebrosidase in neurons derived from Parkinson's disease patients. Nat Commun. 2019;10(1):5570. doi:10.1038/s41467-019-13413-w
12. Kedariti M, Frattini E, Baden P, et al. LRRK2 kinase activity regulates GCase level and enzymatic activity differently depending on cell type in Parkinson's disease. NPJ Parkinsons Dis. 2022;8(1):92. doi:10.1038/s41531-022-00354-3
13. Do J, McKinney C, Sharma P, Sidransky E. Glucocerebrosidase and its relevance to Parkinson disease. Mol Neurodegener. 2019;14(1):36. doi:10.1186/s13024-019-0336-2
14. Gruenberg J. Life in the lumen: The multivesicular endosome. Traffic. 2020;21(1):76-93. doi:10.1111/tra.12715
15. Gallala, H. D., & Sandhoff, K. (2011). Biological function of the cellular lipid BMP-BMP as a key activator for cholesterol sorting and membrane digestion. Neurochemical research, 36(9), 1594–1600. https://doi.org/10.1007/s11064-010-0337-6
16. Alattia JR, Shaw JE, Yip CM, Privé GG. Molecular imaging of membrane interfaces reveals mode of beta-glucosidase activation by saposin C. Proc Natl Acad Sci U S A. 2007;104(44):17394-17399. doi:10.1073/pnas.0704998104
17. Abdul-Hammed M, Breiden B, Schwarzmann G, Sandhoff K. Lipids regulate the hydrolysis of membrane bound glucosylceramide by lysosomal β-glucocerebrosidase. J Lipid Res. 2017;58(3):563-577. doi:10.1194/jlr.M073510
18. Kobayashi T, Stang E, Fang KS, de Moerloose P, Parton RG, Gruenberg J. A lipid associated with the antiphospholipid syndrome regulates endosome structure and function. Nature. 1998;392(6672):193-197. doi:10.1038/32440
19. Matsuo H, Chevallier J, Mayran N, et al. Role of LBPA and Alix in multivesicular liposome formation and endosome organization. Science. 2004;303(5657):531-534. doi:10.1126/science.1092425

20. Mason, R. J., Stossel, T. P., & Vaughan, M. (1972). Lipids of alveolar macrophages, polymorphonuclear leukocytes, and their phagocytic vesicles. The Journal of clinical investigation, 51(9), 2399–2407. https://doi.org/10.1172/JCI107052
21. Huterer, S., & Wherrett, J. (1979). Metabolism of bis(monoacylglycero)phosphate in macrophages. Journal of lipid research, 20(8), 966–973.
22. Bouvier, J., Zemski Berry, K. A., Hullin-Matsuda, F., Makino, A., Michaud, S., Geloën, A., Murphy, R. C., Kobayashi, T., Lagarde, M., & Delton-Vandenbroucke, I. (2009). Selective decrease of bis(monoacylglycero)phosphate content in macrophages by high supplementation with docosahexaenoic acid. Journal of lipid research, 50(2), 243–255. https://doi.org/10.1194/jlr.M800300-JLR200
23. Grabner, G. F., Fawzy, N., Schreiber, R., Pusch, L. M., Bulfon, D., Koefeler, H., Eichmann, T. O., Lass, A., Schweiger, M., Marsche, G., Schoiswohl, G., Taschler, U., & Zimmermann, R. (2020). Metabolic regulation of the lysosomal cofactor bis(monoacylglycero)phosphate in mice. Journal of lipid research, 61(7), 995–1003. https://doi.org/10.1194/jlr.RA119000516
24. Akgoc Z, Sena-Esteves M, Martin DR, Han X, d'Azzo A, Seyfried TN. Bis(monoacylglycero)phosphate: a secondary storage lipid in the gangliosidoses. J Lipid Res. 2015;56(5):1006-1013. doi:10.1194/jlr.M057851
25. Boland S, Swarup S, Ambaw YA, et al. Deficiency of the frontotemporal dementia gene GRN results in gangliosidosis. Nat Commun. 2022;13(1):5924. Published 2022 Oct 7. doi:10.1038/s41467-022-33500-9
26. Goursot A, Mineva T, Bissig C, Gruenberg J, Salahub DR. Structure, dynamics, and energetics of lysobisphosphatidic acid (LBPA) isomers. J Phys Chem B. 2010;114(47):15712-15720. doi:10.1021/jp108361d
27. Alcalay RN, Hsieh F, Tengstrand E, et al. Higher Urine bis(Monoacylglycerol)Phosphate Levels in LRRK2 G2019S Mutation Carriers: Implications for Therapeutic Development. Mov Disord. 2020;35(1):134-141. doi:10.1002/mds.27818
28. Merchant KM, Simuni T, Fedler J, et al. LRRK2 and GBA1 variant carriers have higher urinary bis(monacylglycerol) phosphate concentrations in PPMI cohorts. NPJ Parkinsons Dis. 2023;9(1):30. doi:10.1038/s41531-023-00468-2
29. Gomes S, Garrido A, Tonelli F, et al. Elevated urine BMP phospholipids in LRRK2 and VPS35 mutation carriers with and without Parkinson's disease. NPJ Parkinsons Dis. 2023;9(1):52. doi:10.1038/s41531-023-00482-4
30. Henry AG, Aghamohammadzadeh S, Samaroo H, et al. Pathogenic LRRK2 mutations, through increased kinase activity, produce enlarged lysosomes with reduced degradative capacity

and increase ATP13A2 expression. Hum Mol Genet. 2015;24(21):6013-6028. doi:10.1093/hmg/ddv314

31. Hockey LN, Kilpatrick BS, Eden ER, et al. Dysregulation of lysosomal morphology by pathogenic LRRK2 is corrected by TPC2 inhibition. J Cell Sci. 2015;128(2):232-238. doi:10.1242/jcs.164152
32. de Rus Jacquet A, Tancredi JL, Lemire AL, DeSantis MC, Li WP, O'Shea EK. The LRRK2 G2019S mutation alters astrocyte-to-neuron communication via extracellular vesicles and induces neuron atrophy in a human iPSC-derived model of Parkinson's disease. Elife. 2021;10:e73062. Published 2021 Sep 30. doi:10.7554/eLife.73062
33. Albanese F, Mercatelli D, Finetti L, et al. Constitutive silencing of LRRK2 kinase activity leads to early glucocerebrosidase deregulation and late impairment of autophagy in vivo. Neurobiol Dis. 2021;159:105487. doi:10.1016/j.nbd.2021.105487
34. Kowal J, Arras G, Colombo M, et al. Proteomic comparison defines novel markers to characterize heterogeneous populations of extracellular vesicle subtypes. Proc Natl Acad Sci U S A. 2016;113(8):E968-E977. doi:10.1073/pnas.1521230113
35. Mathieu M, Névo N, Jouve M, et al. Specificities of exosome versus small ectosome secretion revealed by live intracellular tracking of CD63 and CD9. Nat Commun. 2021;12(1):4389. Published 2021 Jul 19. doi:10.1038/s41467-021-24384-2
36. Lu A, Hsieh F, Sharma BR, Vaughn SR, Enrich C, Pfeffer SR. CRISPR screens for lipid regulators reveal a role for ER-bound SNX13 in lysosomal cholesterol export. J Cell Biol. 2022;221(2):e202105060. doi:10.1083/jcb.202105060
37. Fuji RN, Flagella M, Baca M, et al. Effect of selective LRRK2 kinase inhibition on nonhuman primate lung. Sci Transl Med. 2015;7(273):273ra15. doi:10.1126/scitranslmed.aaa3634
38. Baptista MAS, Merchant K, Barrett T, et al. LRRK2 inhibitors induce reversible changes in nonhuman primate lungs without measurable pulmonary deficits. Sci Transl Med. 2020;12(540):eaav0820. doi:10.1126/scitranslmed.aav0820
39. Jennings D, Huntwork-Rodriguez S, Henry AG, et al. Preclinical and clinical evaluation of the LRRK2 inhibitor DNL201 for Parkinson's disease. Sci Transl Med. 2022;14(648):eabj2658. doi:10.1126/scitranslmed.abj2658
40. Lu A, Wawro P, Morgens DW, Portela F, Bassik MC, Pfeffer SR. Genome-wide interrogation of extracellular vesicle biology using barcoded miRNAs. Elife. 2018;7:e41460. Published 2018 Dec 17. doi:10.7554/eLife.41460
41. Body DR, Gray GM. The isolation and characterisation of phosphatidylglycerol and a structural isomer from pig lung. Chem Phys Lipids. 1967;1:254-263.

42. Yadavalli N and Fergusson SM. 2022. LRRK2 Suppresses Lysosome Degradative Activity in Macrophages and Microglia via Transcription Factor E3 Inhibition. doi: https://doi.org/10.1101/2022.12.17.520834
43. Rabia M, Leuzy V, Soulage C, et al. Bis(monoacylglycero)phosphate, a new lipid signature of endosome-derived extracellular vesicles. Biochimie. 2020;178:26-38. doi:10.1016/j.biochi.2020.07.005
44. Wubbolts R, Leckie RS, Veenhuizen PT, et al. Proteomic and biochemical analyses of human B cell-derived exosomes. Potential implications for their function and multivesicular body formation. J Biol Chem. 2003;278(13):10963-10972. doi:10.1074/jbc.M207550200
45. Laulagnier K, Motta C, Hamdi S, et al. Mast cell- and dendritic cell-derived exosomes display a specific lipid composition and an unusual membrane organization. Biochem J. 2004;380(Pt 1):161-171. doi:10.1042/BJ20031594
46. White IJ, Bailey LM, Aghakhani MR, Moss SE, Futter CE. EGF stimulates annexin 1-dependent inward vesiculation in a multivesicular endosome subpopulation. EMBO J. 2006;25(1):1-12. doi:10.1038/sj.emboj.7600759
47. Hsu C, Morohashi Y, Yoshimura S, et al. Regulation of exosome secretion by Rab35 and its GTPase-activating proteins TBC1D10A-C. J Cell Biol. 2010;189(2):223-232. doi:10.1083/jcb.200911018
48. Vieira OV. Rab3a and Rab10 are regulators of lysosome exocytosis and plasma membrane repair. Small GTPases. 2018;9(4):349-351. doi:10.1080/21541248.2016.1235004
49. Bae EJ, Kim DK, Kim C, et al. LRRK2 kinase regulates α-synuclein propagation via RAB35 phosphorylation. Nat Commun. 2018;9(1):3465. Published 2018 Aug 27. doi:10.1038/s41467-018-05958-z
50. Bae EJ, Lee SJ. The LRRK2-RAB axis in regulation of vesicle trafficking and α-synuclein propagation. Biochim Biophys Acta Mol Basis Dis. 2020;1866(3):165632. doi:10.1016/j.bbadis.2019.165632
51. Settembre C, Fraldi A, Medina DL, Ballabio A. Signals from the lysosome: a control centre for cellular clearance and energy metabolism. Nat Rev Mol Cell Biol. 2013;14(5):283-296. doi:10.1038/nrm3565
52. Tsunemi T, Perez-Rosello T, Ishiguro Y, et al. Increased Lysosomal Exocytosis Induced by Lysosomal Ca2+ Channel Agonists Protects Human Dopaminergic Neurons from α-Synuclein Toxicity. J Neurosci. 2019;39(29):5760-5772. doi:10.1523/JNEUROSCI.3085-18.2019

53. Carpenter AE, Jones TR, Lamprecht MR, et al. CellProfiler: image analysis software for identifying and quantifying cell phenotypes. Genome Biol. 2006;7(10):R100. doi:10.1186/gb-2006-7-10-r100
54. Liu N, Tengstrand EA, Chourb L, Hsieh FY. Di-22:6-bis(monoacylglycerol)phosphate: A clinical biomarker of drug-induced phospholipidosis for drug development and safety assessment. Toxicol Appl Pharmacol. 2014;279(3):467-476. doi:10.1016/j.taap.2014.06.014

FIGURE LEGENDS:

Figure 1. **Alterations of antibody-accessible BMP and endo-lysosomal morphology in LRRK2 R1441G-MEF cells. (A)** Confocal microscopy of endogenous BMP (green) and LAMP2 (red) immunofluorescence in WT and R1441G LRRK2 mutant MEF cells. Scale bar: 20µm. **(B-C)** Quantification of vesicular BMP intensity (**B**) and LAMP2 relative intensity (**C**) per cell area. Colored dots represent mean value from 4 independent experiments and violin plots show the distribution of individual cell data. Significance determined by two-tailed paired *t* test **p<0.01, ***p<0.001. **(D)** Representative transmission electron microscopy (TEM) images of Multivesicular endosomes (MVE) from WT and R1441G LRRK2 mutant MEF cells. MVB periphery highlighted in yellow. Scale bar: 250nm. **(E)** MVE area (μm^2) quantification in WT and R1441G LRRK2 mutant cells. Colored dots represent mean values from 3 independent experiments and violin plots show the distribution of individual cell data (35-45 cells/group). **(F)** Quantification of Intraluminal Vesicles (ILVs) per MVE in WT and R1441G mutant MEF cells. The number of ILVs per MVE are binned in three groups and plotted as a percentage of MVE from the total population of each experiment independently. Data from 3 independent experiments (mean ± SEM). Significance determined by two-tailed unpaired *t* test **(E)** and ordinary two-way ANOVA, uncorrected Fisher's LSD **(F)** *p<0.05, ****p<0.0001.

Figure 2. **LRRK2 and GCase activities modulate extracellular vesicle production. (A)** Whole cell lysates from WT and R1441G mutant MEF cells treated with 200nM MLi-2 for 24h were analyzed by western blotting. Representative images of LAMP2, phospho-Rab10 and α-Tubulin levels are shown. Molecular weight marker mobility is shown in kDa. **(B)** Flow cytometry measurement of GCase activity using PFB-FDGlu fluorescent GCase substrate in WT and R1441G LRRK2 mutant MEF cells treated with 300µM CBE for 24h. **(C-D)** Whole cell lysates (WCL) and isolated exosomes from WT and R1441G LRRK2 mutant MEF cells treated with 200nM MLi-2 **(C)** or 300µM CBE **(D)** for 48h were analyzed by western blotting. Representative images of LAMP2, Flotillin1 and α-Tubulin levels are shown. Molecular weight marker mobility is shown in kDa. **(E-G)** Quantification of LAMP2 and Flotillin1 levels relative to R1441G LRRK2 MEF cells in whole cell lysates (WCL). **(E)** and isolated exosomes **(F-G).** Data

from 6-9 independent experiments (mean ± SEM). Significance determined by two-tailed paired *t* test compared to R1441G LRRK2 control *p<0.05, **p<0.01, ****p<0.0001.

Figure 3. **Targeted lipid pathway analysis of BMP abundance in cellular and isolated exosomal fractions. (A-D)** UPLC-MS/MS determination of BMP isomers normalized to protein content from cells treated with 200nM MLi-2 **(A-B)** or 300µM CBE **(C-D)** for 48h. Data shown as fold change relative to R1441G LRRK2 control MEF cells. Only BMP isomers that were detected are shown. **(E)** UPLC-MS/MS determination of BMP isomers normalized to protein content in exosomes isolated from cells treated with 200nM MLi-2 or 300µM CBE for 48h. Only BMP isomers that were detected are shown. Data from 3-6 independent experiments (mean ± SEM). Significance determined by ordinary one-way ANOVA, uncorrected Fisher's LSD **(A-D)** and one-way ANOVA with the Geisser-Greenhouse correction, uncorrected Fisher's LSD **(E)** *p<0.05, **p<0.01, ***p<0.001, ****p<0.0001.

Figure 4. **Inhibition of LRRK2 or GCase activities does not significantly impact BMP biosynthetic and catabolic rates. (A)** Schematic representation of the BMP metabolic labeling protocol with deuterated docosahexaenoic acid and ^{13}C-labeled oleic acid. WT and R1441G mutant MEF cells were incubated with a pulse of DHA-d5 / OA-^{13}C for 20min, followed by a chase for different times. Cells were then collected for subsequent BMP lipidomic analysis. Structures of unlabeled (L) and isotope-labeled (H) fatty acids are shown in black or red, respectively. **(B-D)** UPLC-MS/MS determination of BMP isomers normalized to protein content from WT MEF cells and R1441G LRRK2 mutant MEF cells ± MLi-2 (200nM) or CBE (300µM). Long **(B-C)** and short **(D)** chase time points shown as fold change relative to WT control MEF cells time 0. Only BMP isomers that were detected are shown. Data from 3 replicated experiments (mean ± SEM).

Figure 5. **Pharmacological modulation of exosome-mediated BMP exocytosis. (A)** Whole cell lysates (WCL) and isolated exosomes from WT MEF cells treated with 10µM GW4869 or 10nM bafilomycin-A1 (B-A1) for 24h were analyzed by western blotting. Representative images of LAMP2, Flotillin1 and α-Tubulin levels are shown. Molecular weight marker mobility is shown in kDa. **(B-C)** UPLC-MS/MS determination of BMP isomers normalized to protein content from WT MEF cells treated with 10nM B-A1 **(B)** or 10µM GW4869 **(C)** for 24h. Data shown as fold change relative to WT control MEF cells. Only BMP isomers that were detected are shown. Data from 6 independent experiments (mean ± SEM). Significance determined by two-tailed unpaired *t* test *p<0.05, **p<0.01, ***p<0.001, ****p<0.0001. **(D-E)** Quantitation of BMP isomers normalized to protein content in exosomes isolated from MEF WT cells treated with 10nM B-A1 **(D)** or 10µM GW4869 **(E)** for 24h. Data shown as fold change relative to WT control MEF cells. Only BMP isomers that were detected are shown. Data from 3

independent experiments (mean ± SEM). Significance determined by two-tailed unpaired *t* test *p<0.05, **p<0.01, ***p<0.001.

Supplemental Figure 1. **No significant differences in exosome release and cellular or exosome-associated BMP levels between MLi-2/CBE–treated and untreated WT MEF cells. (A-C)** Quantification of LAMP2 and Flotillin1 levels relative to WT control MEF cells in WCL **(A)** and isolated exosomes **(B-C).** Data from 7-8 independent experiments (mean ± SEM). Significance determined by ordinary one-way ANOVA, uncorrected Fisher's LSD. **(D-F)** UPLC-MS/MS measurements of cellular **(D-E)** and exosome-associated **(F)** BMP isomers normalized to protein content from cells treated with 200nM MLi-2 or 300µM CBE for 48h or left untreated (ctrl). Data shown as fold change relative to WT control MEF cells. Only BMP isomers that were detected are shown. Data from 6-7 independent experiments (mean ± SEM). Significance determined by ordinary two-tailed paired *t* test.

Supplemental Figure 2. **Quantitative analysis of GCase substrates in MEF cells and exosomal fractions. (A-B)** Lipidomic determination of Glucosylceramide (GlcCer), Galactosylceramide (GalCer) and Glucosylsphingosine (GlcSph) isomers normalized to protein content from WT and R1441G LRRK2 mutant MEF cells **(A)** and isolated exosomes **(B)** treated with 300µM CBE or 200nM MLi-2 for 48h. Heatmap showing values as fold change relative to R1441G LRRK2 mutant MEF cell control. Only GlcCer, GalCer and GlcSph isomers that were detected are shown. Data from 3-9 independent experiments (mean ± SEM). Significance determined by ordinary two-way ANOVA, uncorrected Fisher's LSD *p<0.05, **p<0.01, ***p<0.001 ****p<0.0001.

Supplemental Figure 3. **Pharmacological modulation of exosome-mediated BMP exocytosis in mutant LRRK2 MEF cells .** Whole cell lysates (WCL) and isolated exosomes from R1441G LRRK2 MEF cells treated with 10µM GW4869 or 10nM bafilomycin-A1 for 24h were analyzed by western blotting. Representative images of LAMP2, Flotillin1 and α-Tubulin levels are shown. Molecular weight marker mobility is shown in kDa.

MATERIALS AND METHODS:

Cell culture, antibodies and other reagents–Wild type (WT) and R1441G LRRK2 mutant MEF cells were grown in Dulbecco's modified Eagle's media (DMEM) containing 10% fetal bovine serum, 2 mM L-glutamine, and penicillin (100 U/ ml)/streptomycin (100 mg/ml). Cell lines were cultured at 37˚C with 5% CO2. Extracellular vesicle-free media was prepared by overnight ultracentrifugation of DMEM or RPMI supplemented with 10% FBS at 100,000 X g in a SW32Ti rotor. For bafilomycin-A1 (Sigma-Aldrich; catalog no. B1793) and GW4869

(SelleckChem; catalog no. S7609), the drug was added to cell media at 10 nM and 10 µM respectively and cells were cultured for 24 h before exosome collection. For MLi-2 (Tocris Bioscience; catalog no. 5756) and Conduritol B Epoxide (MERK; catalog no. 234599), the drug was added to cell media at 200nM and 300µM respectively and cells were cultured for 48 h before exosome isolation. 0.167mM Oleic acid (Cambridge Isotope Laboratories; catalog no. DLM-10012-0.001) and Docosahexaenoic acid (Cambridge Isotope Laboratories; catalog no. DLM-10012-0.001) were conjugated with 0.0278mM fatty acid–free BSA (Sigma-Aldrich; A8806) at a 1:6 molar ratio. Primary antibodies diluted in PBS with 1% BSA (for immunofluorescence) or 5% skim milk (for immunoblotting) were mouse anti–lysobisphosphatidic acid (anti-BMP) clone 6C4 1:1000 (EMD Millipore; catalog no. MABT837), rat monoclonal anti-mouse LAMP2 1:1000 (Developmental Studies Hybridoma Bank, catalog no.GL2A7), mouse anti-Flotillin1 1:1000 (BD Biosciences; catalog no.610821), rabbit anti-phospho-Rab10 1:1000 (Abcam; catalog no. ab230261), mouse anti-alpha tubulin 1:10000 (SigmaAldrich; catalog no. T5168), mouse anti-Actin 1:5000 (Abcam; catalog no. ab3280).

Immunofluorescence– Wild type (WT) and R1441G LRRK2 mutant MEF cells were fixed with 3.7% (v/v) paraformaldehyde for 15 min, washed and permeabilized/blocked with 0.1% saponin/1% BSA-PBS before staining with anti-LAMP2 and anti-BMP antibodies followed by goat anti-rat AlexaFluor555 and donkey anti-mouse AlexaFluor488. Nuclei were stained using 0.1 mg/ml DAPI (SigmaAldrich; catalog no. D9542). Coverslips were mounted on glass slides with Mowiol. Microscopy images were acquired using a Zeiss LSM880 laser scanning spectral confocal microscope (Carl Zeiss) equipped with an Axio Observer 7 inverted microscope, a blue diode (405 nm), argon (488 nm), diode-pumped solid-state (561 nm), and HeNe (633 nm) lasers, and a Plan Apochromat 63×/NA1.4 oil-immersion objective lens. DAPI, Alexa Fluor 488, Alexa Fluor 555 were acquired sequentially using 405-, 488- and 561-nm laser lines; Acousto-Optical Beam Splitter as a beam splitter; and emission detection ranges 415–480 nm, 500–550 nm, 571–625 nm, respectively. The confocal pinhole was set at 1 Airy unit. All images were acquired in a 1,024 × 1,024–pixel format. BMP and LAMP2 intensities were quantified using CellProfiler[53].

Immunoblotting–Cells were lysed in lysis buffer (50 mM Hepes, 150 mM KCl, 1% Triton X-100, 5 mM MgCl2, pH 7.4) supplemented with a protease/ phosphatase inhibitor cocktail (1mMNa3VO4, 10mMNaF, 1 mM PMSF, 10 µg/ml leupeptin, and 10 µg/ml aprotinin). After centrifugation at 12,000 g for 10 min, protein concentrations were measured in the cleared lysates. Equal amounts were resolved by SDS-PAGE followed by immunoblot analysis. Exosome final pellets were resuspended in SDS-PAGE loading dye (50 mM Tris-HCl pH 6.8, 6% glycerol, 2% SDS, 0.2% bromophenol blue), heated briefly at 95°C, resolved by 10% SDS-PAGE gel and transferred onto nitrocellulose membranes (Bio-Rad Laboratories; catalog no. 1620115) using a Bio-Rad Trans-Blot system. Membranes were blocked with 5% skim milk in TBS withTween-20 for 60 min at RT. Primary antibodies were diluted in blocking buffer and incubated overnight at 4°C. HRP-conjugated secondary antibodies (Bio-Rad Laboratories) diluted in blocking buffer at 1:3000 were incubated for 60 min at RT and developed using EZ-ECL (Biological Industries) or SuperSignal West Femto (Thermo Scientific; catalog no. 34094). Blots were imaged using an ImageQuant LAS 4000 system (GE Healthcare) and quantified using ImageJ software.

Transmission Electron Microscopy–Cells in culture were washed in PBS and fixed for 1h in 2.5% glutaraldehyde in 0.1 M phosphate buffer (PB) at RT. Next, samples were slowly and gently scraped and pelleted in 1.5 ml tubes. Pellets were washed in PB and incubated with 1% OsO4 for 90 min at 4 °C. Then samples were dehydrated, embedded in Spurr and sectioned using Leica ultramicrotome (Leica Microsystems). Ultrathin sections (50–70 nm) were stained with 2% uranyl acetate for 10 min, a lead-staining solution for 5 min and observed using a transmission electron microscope, JEOL JEM-1010 ftted with a Gatan Orius SC1000 (model 832) digital camera. Multivesicular Endosomes (MVE) and Intralumenal Vesicles (ILV) were identified by morphology and MVE area and ILV number were measured using ImageJ.

Exosome isolation–MEF adherent cell cultures were seeded at 3-4*10^6 cells/plate in exosome-free complete DMEM and grown for 24–48 h. Cell cultures were centrifuged at 300 g, 5 min to pellet cells, and supernatants were centrifuged again at 2100 g, 20 min to pellet dead cells. After this, filtration through 0.22 mm filter units was performed. Filtered media were ultracentrifuged for 75 min at 100,000 g in SW32Ti rotor to pellet extracellular vesicles. The supernatant was discarded, and the pellet re-suspended in phosphate-buffered saline (PBS) and centrifuged again for 75 min at 100,000 g in 140AT rotor. exosome pellets were frozen and stored at -80°C prior to further processing.

Lipidomic analysis–Targeted quantitative ultra-performance liquid chromatography tandem mass spectrometry was used to accurately quantitate the three geometrical isomers (2,2-, 2,3- and 3,3-) of di-22:6-BMP and di-18:1-BMP in control or treated MEF cells. Lipidomic analyses were conducted by Nextcea, Inc. as previously described[54]. Standard curves were prepared using authentic BMP reference standards. Protein was determined by bicinchoninic acid protein assay. A multiplexed quantitative ultraperformance liquid chromatography tandem mass spectrometry method was used to simultaneously quantitate sample glucosylceramides (GluCer d18:1/16:0, d18:1/18:0, d18:1/22:0, d18:1/24:0, d18:1/24:1), galactosylceramides (GalCer d18:1/16:0, d18:1/18:0, d18:1/22:0, d18:1/24:0, d18:1/24:1), glucosylsphingosine (GluSph 18:1), and galactosylsphingosine (GalSph 18:1). Standard curves were prepared from related standards using a class-based approach. Internal standards were used for each analyte reported. A SCIEX Triple Quad 7500 mass spectrometer was used in positive electrospray ionization mode for detection (SCIEX, Framingham, MA, USA). Injections were made using a Shimadzu Nexera XR UPLC (ultraperformance liquid chromatography) system (Shimadzu Scientific Instruments, Kyoto, Japan). The instruments were controlled by SCIEX OS 2.0 software.

Metabolic labeling–WT and R1441G LRRK2 mutant MEF cells were treated with 200nM MLi-2 or 300µM CBE for 16h. Cells were washed twice with PBS and incubated in serum-free DMEM ± MLi-2 or CBE for 1h. Incubate cells in 0.167mM 13C-labeled Oleic Acid (OA) and 0.167mM deuterated docosahexaenoic acid (DHA) in serum-free DMEM containing 0.0278mM BSA for 20 min. Cells were washed with serum-free DMEM and chased with serum-free DMEM for short time points (0, 15, 30, 45, 60min) or complete DMEM for long timepoints (8, 24 and 48h). Cells were washed with PBS, trypsinized and collected in cold PBS. Cells were pelleted by centrifugation at 1000rpm for 7min and stored at -80°C prior to further processing.

GCase activity–GCase activity was measured by using the fluorogenic substrate PFB-FDGlu (Invitrogen, Carlsbad, CA). WT and R1441G LRRK2 mutant MEF cells were treated with 300µM CBE for 24h. After this, 150 µg/ml PFB-FDGlu (Thermo Fisher) was then added to cells followed by incubation for 2h at 37°C. Cells were then washed twice with PBS, trypsinized and fixed in cold 2% paraformaldehyde-PBS for 30 min. Cells were washed twice in PBS before assayed on a FACS analyzer (FACScan; BD) equipped with a 488 nm laser and 530 nm-FITC filter. Data were analyzed using Flowjo software (Tree Star).

Statistics–Results are expressed as the mean ± SEM. Means were compared using Student's t test when two experimental conditions were independently compared. Unless otherwise noted, statistical significance between multiple comparisons was assessed via one-way or two-way ANOVA with uncorrected Fisher's LSD test using GraphPad Prism version 9.

Figure 1 Meneses-Salas et al.

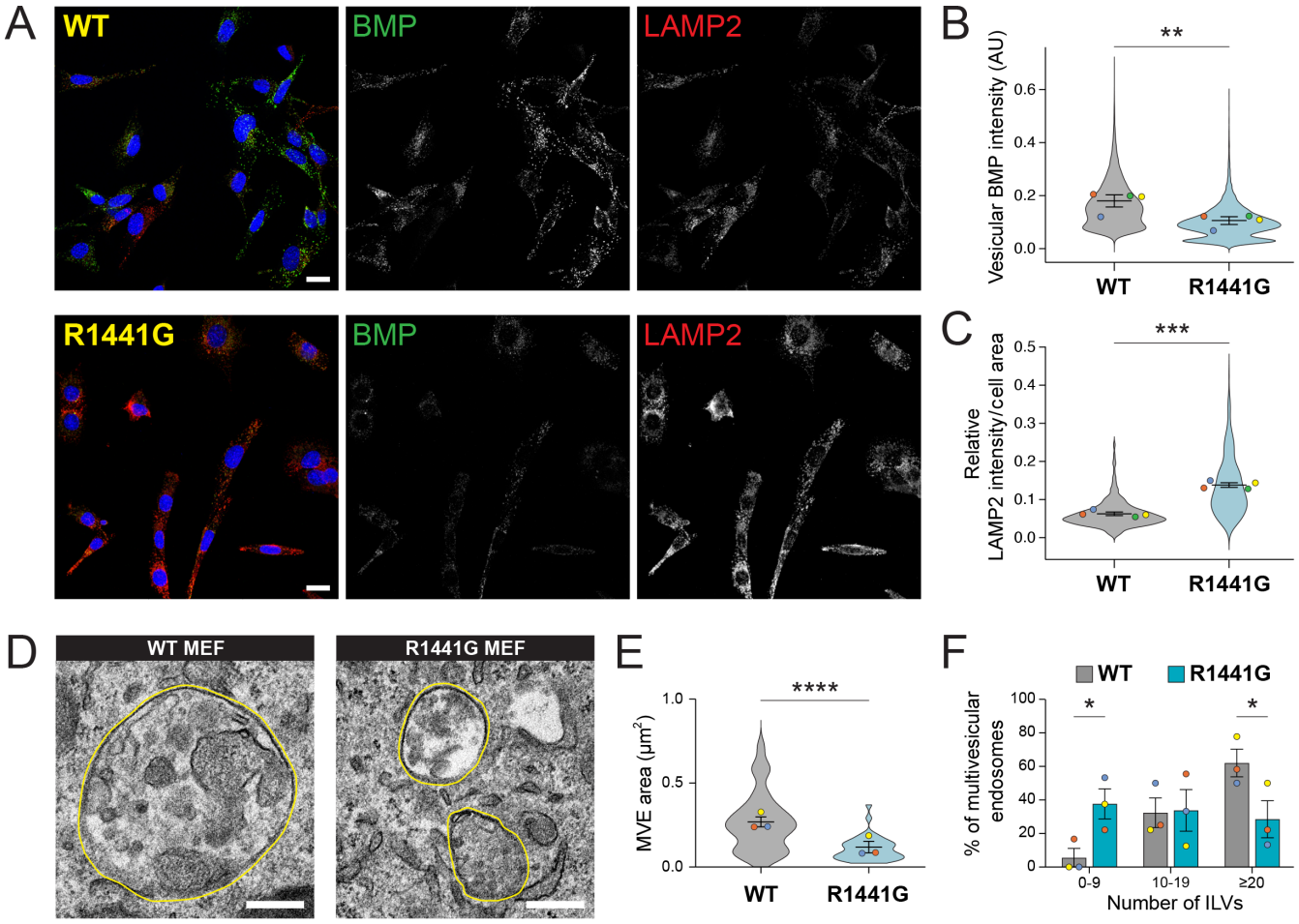

Figure 2 Meneses-Salas et al.

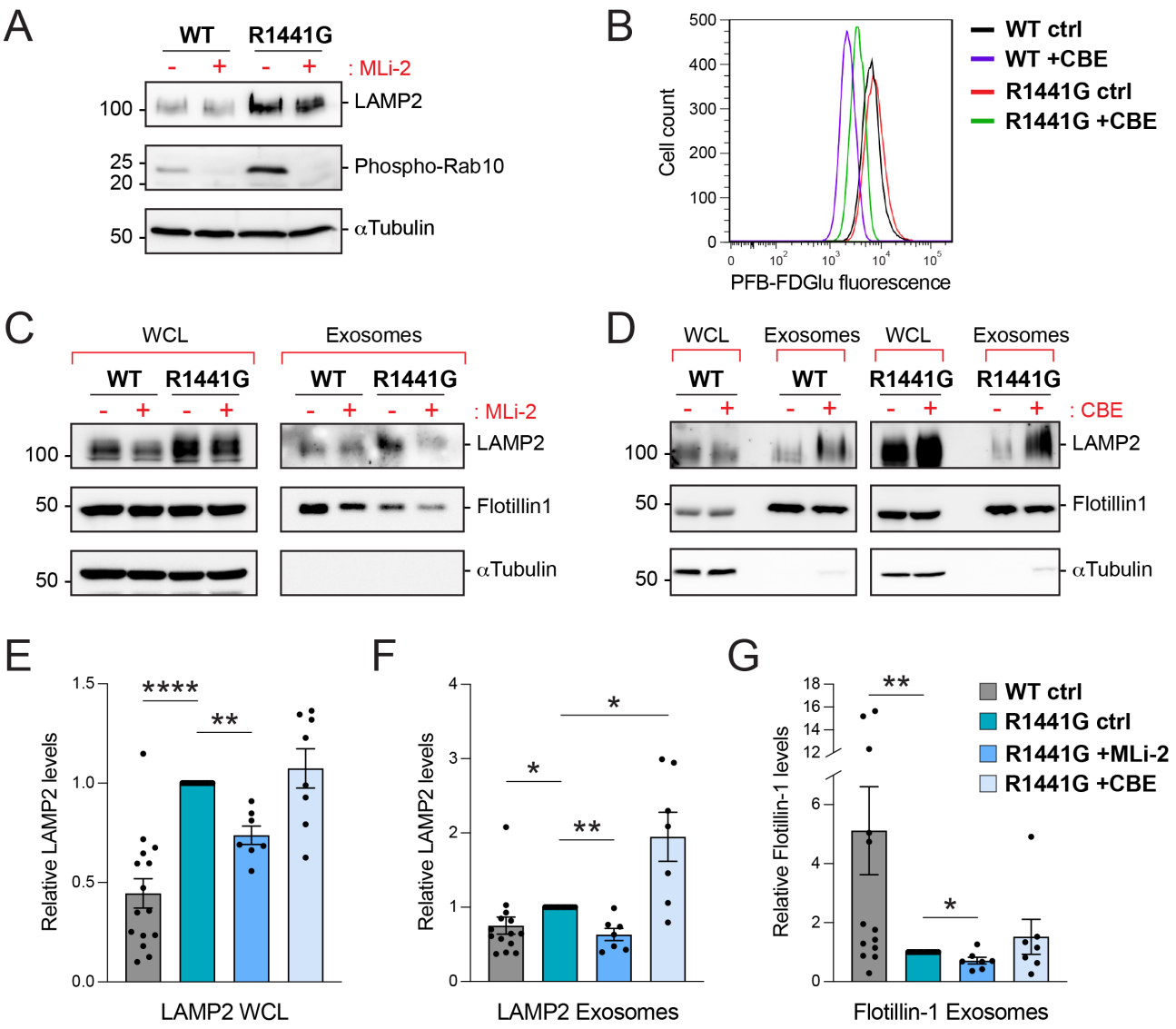

Figure 3 Meneses-Salas et al.

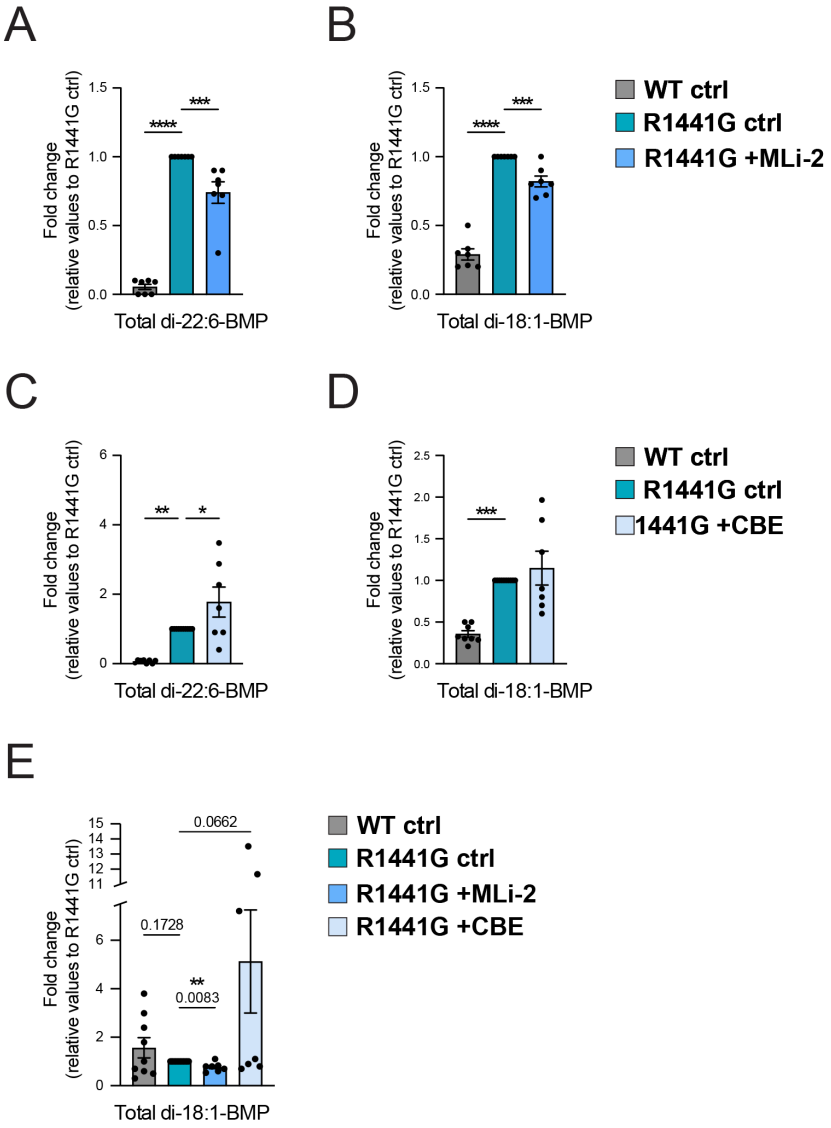

Figure 4 Meneses-Salas et al.

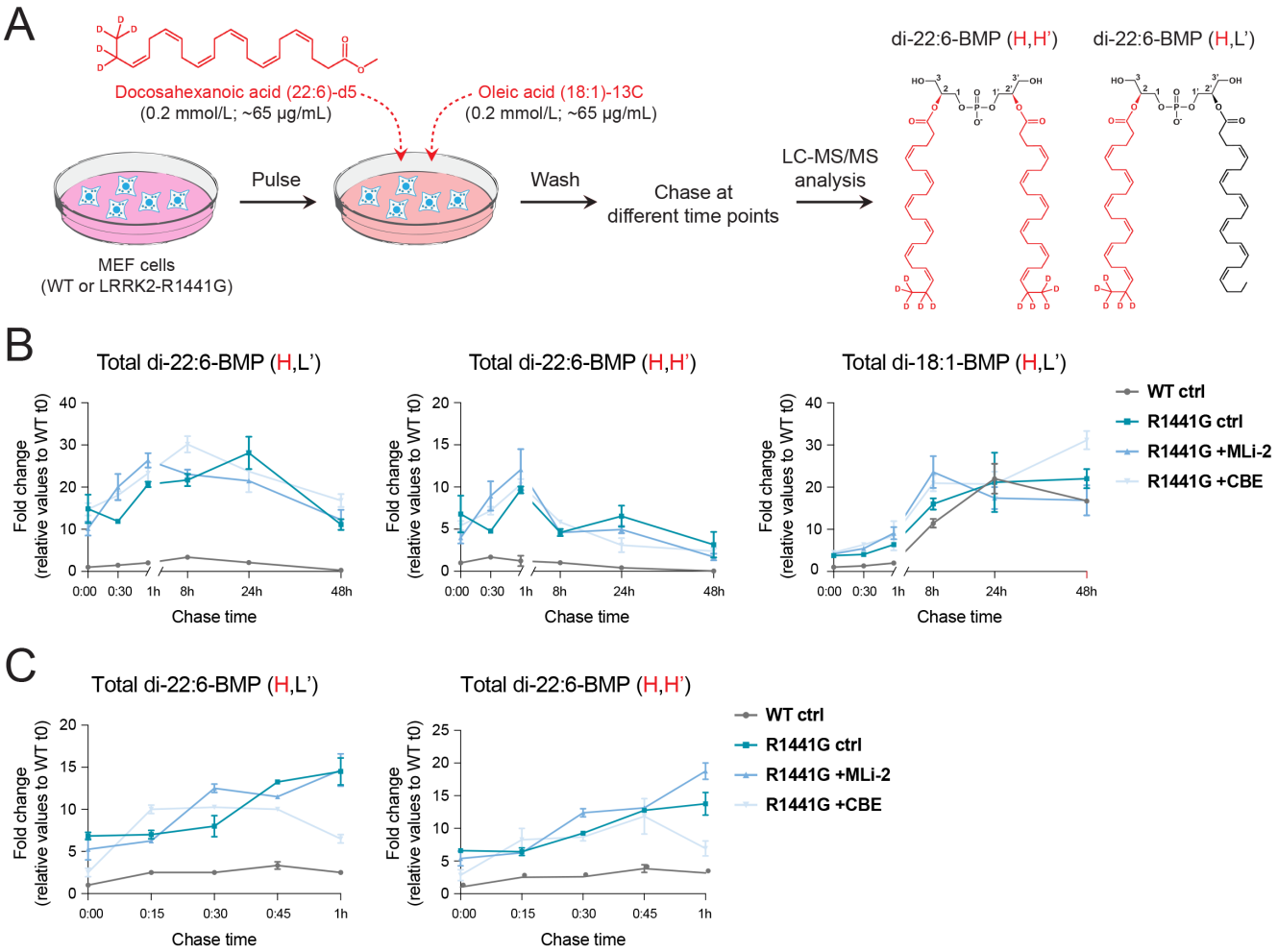

Figure 5 Meneses-Salas et al.

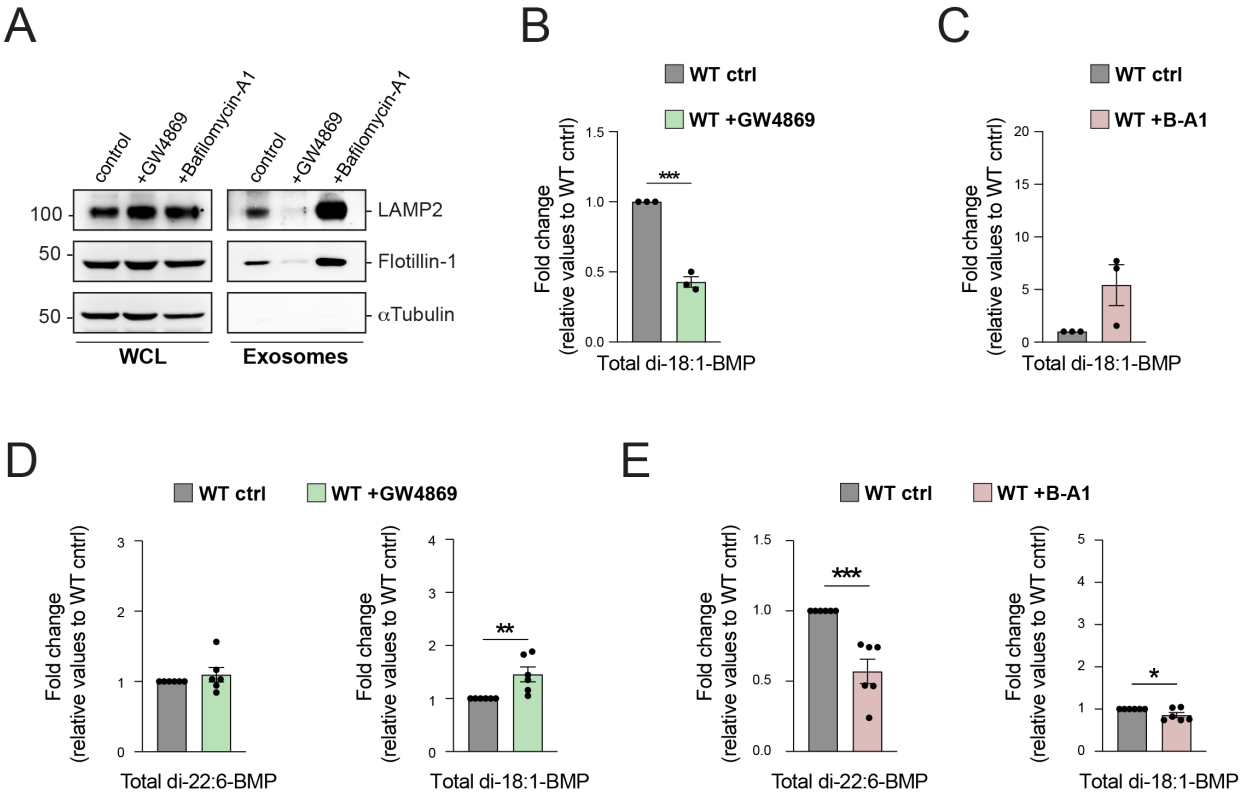

Supplemental Figure 1 Meneses-Salas et al.

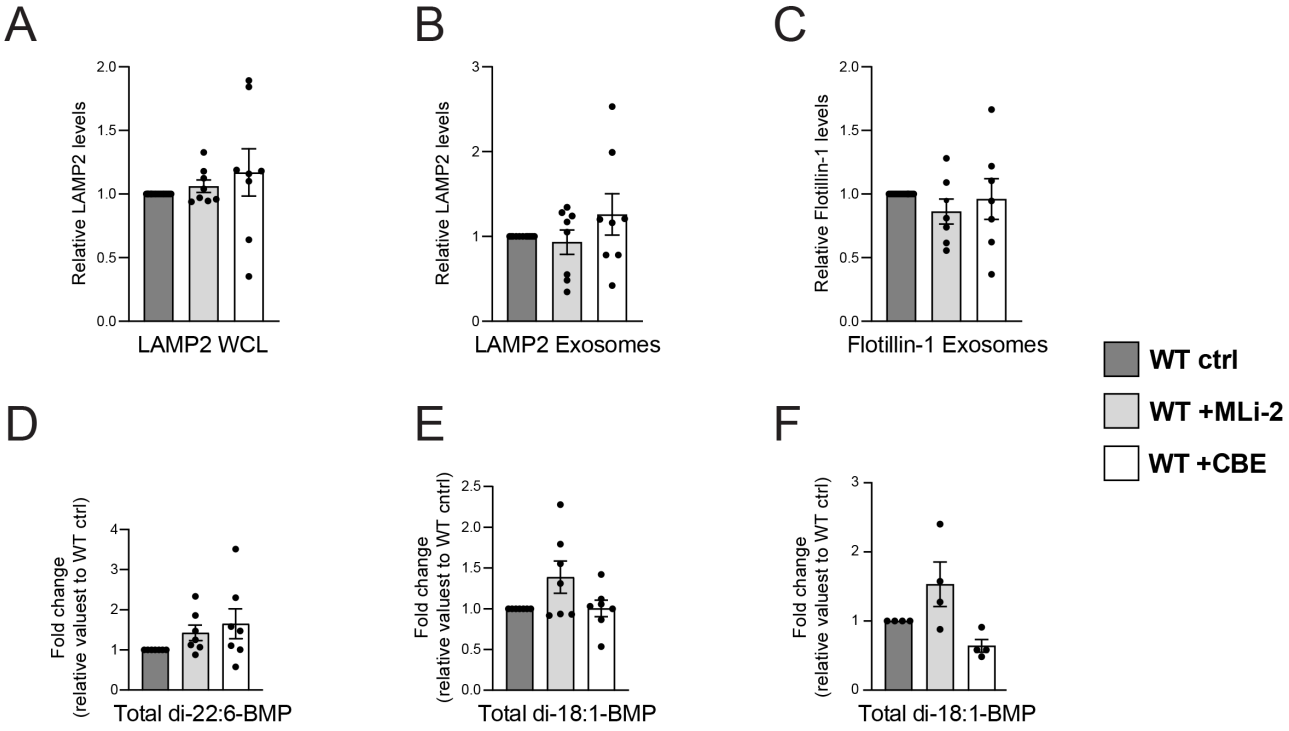

Supplemental Figure 2 Meneses-Salas et al.

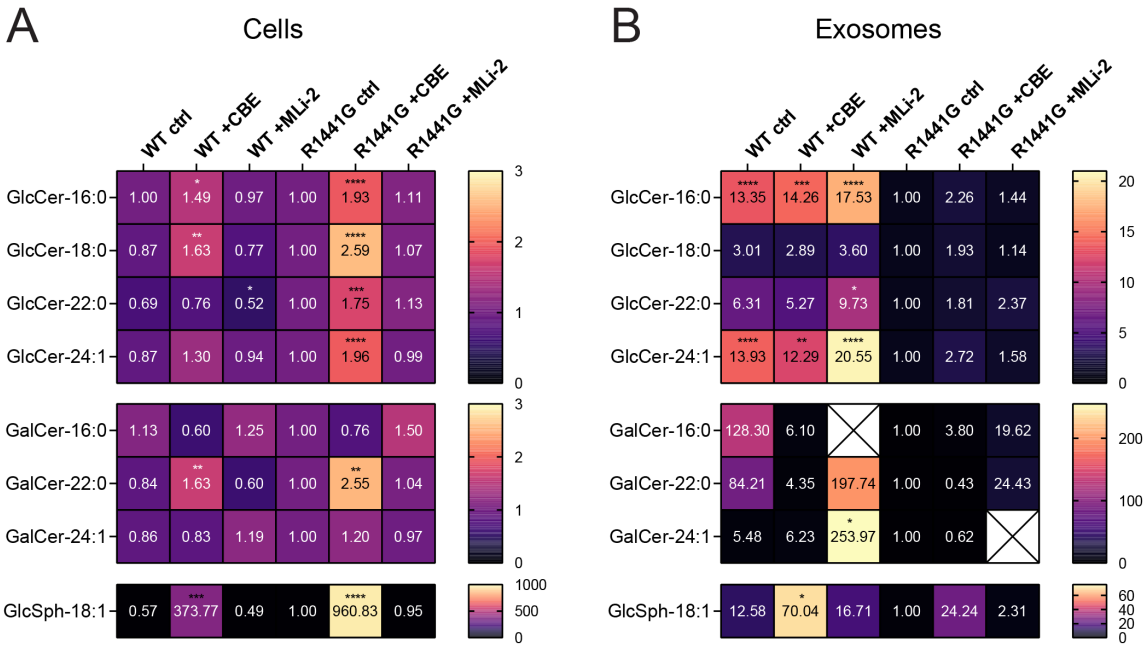
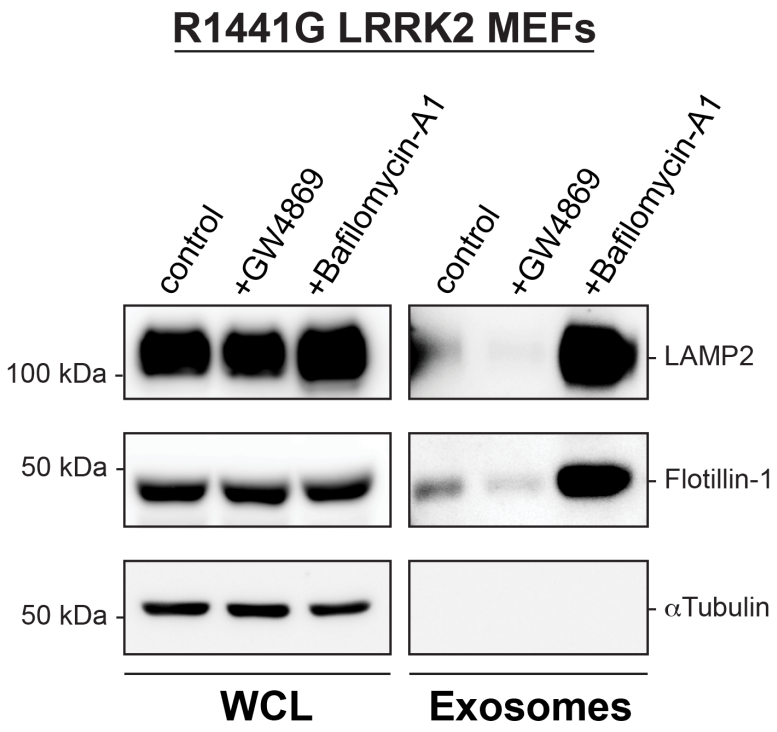
Supplemental Figure 3 Meneses-Salas et al.